An algorithm for retrieval albedo from BRDF archetype

ZHANG Hu, JIAO Ziti, DONG Yadong, HUANG Xingying, LI Jiayue, LI Xiaowen

1. *School of Geography, Beijing Normal University, Beijing* 100875, *China*;
2. *State Key Laboratory of Remote Sensing Science, jointly spansored by Beijing Normal University and Institute of Remote Sensing and Digital Earth, Chinese Academy of Sciences, Beijing* 100875, *China*;
3. *Key Laboratory of Environmental Remote Sensing and Digital City, Beijing Normal University, Beijing* 100875, *China*

Abstract: A priori knowledge plays an important role in the retrieval of surface albedo from satellite observations. Here a BRDF archetype database is built according to Anisotropic Flat Index (AFX) which can identify surface reflectance anisotropy. Then a method to derive land surface albedo from spare observations and BRDF archetype is presented. Albedos from all the observations and full inversion method are used to validate the albedo estimation from our method. Compared results show that, when the observations that have view zenith angles less than 40° are not on the cross-principle plane can only represent part of reflectance anisotropy. Compared with full inversion method, the maximum absolute error of BRDF archetype inversion method is 0.036, and the relative error is improved about 5%—10%. For those observations are located on the cross-principle plane, the largest absolute difference of full inversion method is up to 0.18 due to the insufficient and spare angular samples. However, the BRDF archetype inversion method appears more accurate. In sum, BRDF archetype inversion method constrains BRDF shape over the entire space and was less dependent on the distribution of the observations. It was also less sensitive to noise. For the multi-angle data that have insufficient information, BRDF archetype method is preferred than full inversion method.

Key words: AFX, BRDF archetype, archetype inversion, full inversion, albedo

CLC number: TP701 **Document code:** A

Citation format: Zhang H, Jiao Z T, Dong Y D, Huang X Y, Li J Y and Li X W. 2013. An algorithm for retrieval albedo from BRDF archetype. Journal of Remote Sensing, 17(6): 1475-1491 [DOI: 10.11834/jrs.20133022]

1 INTRODUCTION

Anisotropic character is an inherent behavior of Land surface reflectance, and this property is usually characterized by the Bidirectional Reflectance Distribution Function (BRDF) (Nicodemus, et al., 1977). Surface albedo, which can be produced through the integration of BRDF, is defined as the ratio of the reflected solar ration to the total incoming solar radiation over the whole solar spectrum (Dickinson, 1983). It is the ability of surface to reflect solar radiation and is also used as an input parameter for climate models, and thus it is a primary controlling for the surface energy budget (Dickinson, 1985). Access of high accuracy of surface albedo has great significance to global climate change research.

The anisotropic characteristics of the surface should be considered when quantitative estimation of surface albedo and features of vegetation and soil from surface direction reflectance (Li & Wang, 1995). The linear kernel driven BRDF model which has the ability of integration and extrapolation is generally used in correcting BRDF effects and in the retrieval of surface albedo from multi-angle datasets (Lucht, et al., 2000; Schaaf, et al., 2002; Strugnell & Lucht, 2001). However the acquisition of angular measurements from the sensor is limited by its scanning configuration and the platform's orbital characteristics. Moreover, cloud contamination reduces the number of observations and makes the angular distribution hard to predict. Most multi-angle samplings (e.g. MODIS) are accumulated during certain period based on an assumption that the BRDF character of the land surface remains unchanged during this period (Jin, et al., 2003; Schaaf, et al., 2002). Sun zenith angle, meteorological situation and surface conditions can cause great variance in directional reflectance. They have more obvious effect in high resolution remote sensing, because high resolution sensors can only cover a small region and they can not get enough samplings in a short time. Moreover, the kernel driven model has a strict set of rules for the number and distribution of observations (Jin, et al., 2003). All the factors mentioned above can limit the retrieval accuracy of the surface albedo.

A priori knowledge can effectively solve the problem of insufficient number of observations in the inversion of remote sensing. In existing algorithms using a priori knowledge usually assume that the same land surface has a similar BRDF shape,

Received: 2013-01-28; **Accepted:** 2013-05-27; **Version of record first published:** 2013-06-03

Foundation: National High Technology Research and Development Program of China (863 Program) (No. 2012AA12A304); National Natural Science Foundation of China (No. 41171261, 40871193)

First author biography: ZHANG Hu (1986—), male, Ph. D. candidate, he majors in the application of quantitative remote sensing, surface bidirectional reflectance and surface albedo. E-mail: askzhanghu@126.com

Corresponding author biography: JIAO Ziti (1970—), male, associate professor. His research interests are modeling reflectance anisotropy and albedo, and differentiating land covers with multiple-view-angle remotely sensed data. E-mail: jiaozt@bnu.edu.cn

and the optimal BRDF shape of the data can be got through fitting the priori BRDF shape to observations (Strugnell & Lucht, 2001). However, there are also studies showed that the variability of BRDF is higher within the class than between the class (Bacour & Bréon, 2005). This may be because BRDF is directly related to vegetation structure (Li & Strahler, 1985; 1992; Strahler & Jupp, 1990), and different land covers may have the same structure. Moreover, the degree of spatial heterogeneity changes only slightly beyond 1 km resolution and the BRDF shapes are similar (Bacour & Bréon, 2005). Spatial heterogeneity characteristics will increase when pixel size is reduced, and BRDF shape will change obviously with the variance of vegetation structure (Roman, et al., 2011).

The present study first uses kernel driven BRDF model (RossThick-LiSpareR) (Wanner, et al., 1995) to fit surface observation data, and then establishes the BRDF archetype database according to Anisotropic Flat Index (AFX) calculated from model parameters. Then we introduce an algorithm for retrieval albedo from insufficient observations using the BRDF archetypes. Finally simulated data is used to analyze the accuracy of the result through comparing this method with MODIS albedo full inversion method (Lucht, et al., 2000). The advantages of this method and the sources of error are also discoursed.

2 DATA AND ALGORITHM BASIS

2.1 Multi-angle data set

The major advantage of ground multi-angular observation is the ability to acquire various directional reflectance of the same feature in a short time, which may be helpful for land surface reflectance anisotropy. The 73 sets of field observations used in this study contained a large number of plant covers, for instance, soil, grass, shrub, broadleaf crops and forests. Most of the data sets are collected on the ground and used in many studies (Kimes, 1983, 1986; Ranson, 1985; Deering, 1986; 1992; 1999; Irons, 1992; Vierling, 1997). There are also some airborne POLDER data sets (Leroy & Breon, 1996) and Scanning Cloud Absorption Radiometer (SCAR) observations (Tsay, et al., 1998). These datasets are acquired in the red and near infrared bands, most of which are used for validating the models´ fitting capability (Li, et al., 2001; Hu, et al., 1997). Detail information of each data can refer to Huang (2013).

2.2 Algorithm theoretical basis

2.2.1 Kernel driven BRDF model

Land surface reflectance anisotropy has been widely accepted, and directional reflectance can be described according to a function of the sun and the view angle. Kernel driven BRDF model, which is a linear combination of some base kernels, is generally used to the retrieval of surface albedo. For non-Lambert pixels, directional reflectance can be divided into a linear combination of isotropic scattering, volume scattering and geometrical optics scattering (Lucht, et al., 2000; Roujean, et al., 1992; Wanner, et al., 1995).

$$R(\theta_i,\theta_r,\varphi) = f_{iso}(\lambda) + f_{vol}(\lambda)K_{vol}(\theta_i,\theta_r,\varphi) + f_{geo}(\lambda)K_{geo}(\theta_i,\theta_r,\varphi) \quad (1)$$

where R is the surface bidirectional reflectance, and K_{vol} represents the volume scattering kernel caused by a horizontal layer of randomly distribution leaves, and K_{geo} represent the s urface scattering kernel caused by shadows of natural objects. They are the functions of viewing and illumination geometry; θ_i, θ_r, and φ are the solar zenith, view zenith and relative azimuth angles, respectively; $f_{iso}(\lambda)$, $f_{vol}(\lambda)$, $f_{geo}(\lambda)$ are the spectrally dependent BRDF kernel weights or parameters.

MODIS full inversion method uses the linear regression to fit observations and retrieves the best model parameters. During the retrieval of albedo from observations, a constraint method is considered to avoid negative non-physical BRDF parameters (Jin, et al., 2003). The value of kernel integration has nothing to do with model parameter, and can be calculated in advance. Black Sky Albedo (BSA) and White Sky Albedo (WSA) can be retrieved through the linear combination of multiple values of model parameters and kernel volume (Lucht, et al., 2000). Actual albedo is a value interpolated between WSA and BSA on the diffuse skylight fraction (Lewis & Barnsley, 1994). A large number of studies showed that when the observations can represent the surface anisotropy, the full inversion results performed consistently with field observations (Jin, et al., 2003; Liu, et al., 2009; Schaaf, et al., 2002).

The RossThick and LiSparse-Reciprocal (RTLSR) kernels (Wanner, et al., 1995) are used in this research. Their BRDF shapes on the principle plane at different view zenith angles are shown in Fig. 1. The RossThick kernel presents a typical bowl-

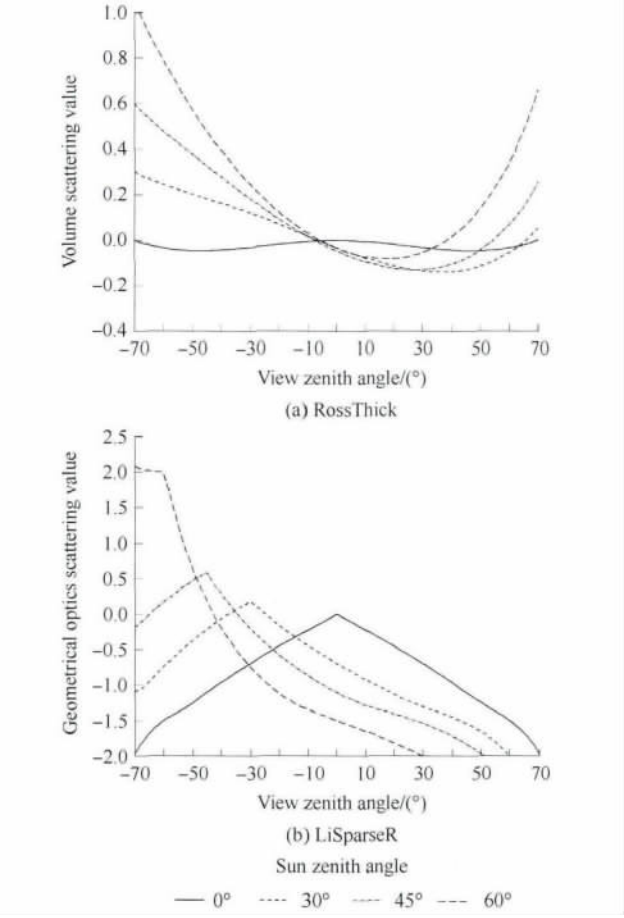

Fig. 1 The BRDF shape on the principle plane at different sun zenith angle

shaped BRDF curve where reflectance near nadir is lower than for larger scattering angle with the minimum usually displaced towards the forward scattering direction while the reciprocal LiSparse kernel presents dome-shaped BRDF curve with prominent peak reflectance (hotspot) in retro-solar direction. Actual BRDF shapes are combined by these two basic shapes, so it is fair to believe that the actual BRDF will exhibit bowl or dome shape character on some degree.

2.2.2 Anisotropic Flat indeX (AFX)

AFX has a formula derived from the kernel-driven BRDF model (Eq. (2)) and is especially appropriate for the description of the MODIS anisotropic reflectance. It is defined as the ratio of WSA to the isotropic parameter f_{iso}

$$\mathrm{AFX} = \frac{\mathrm{WSA}(\Lambda)}{f_{iso}(\Lambda)} \quad (2)$$

The value of AFX depends on the band Λ. Based on the RTLSR BRDF model, we derive the AFX as Eq. (3):

$$\mathrm{AFX} = 1 + \frac{f_{vol}(\Lambda)}{f_{iso}(\Lambda)} \times 0.189184 - \frac{f_{geo}(\Lambda)}{f_{iso}(\Lambda)} \times 1.377622 \quad (3)$$

where constant 0.189184 and 1.377622 are the bi-hemispherical integral of the RossThick kernel and reciprocal LiSparse kernel, respectively.

From Eq. (3), we can see that AFX is a linear combination of the volumetric parameter and geometric-optical parameter normalized by isotropic parameter, and weighted by bi-hemispherical integral value of the RossThick kernel and the LiSparse-Reciprocal kernel respectively. AFX varies as the geometric-optical and volumetric parameters. If the volumetric scattering effect is greater than the geometric-optical effect, then an AFX > 1 is expected; if the geometric-optical effect is greater than volumetric effect, an AFX < 1 is expected; otherwise, an AFX ≈ 1 is available. The level of the surface reflectance depends on the band. Bare land is the typical soil background land cover type, and they have a similar level of reflectance in the red and near-infrared bands. However, for the dense vegetation, there are significant reflectance gaps between those two bands. The reflectance level of grass and shrub land is between those two land covers. The original BRDF (gray line in Fig. 2) retrieved from observations contains the anisotropic information as well as the spectral information of land surface, thus, these BRDF shapes do not present distinctly regular variability and are hard to use in research. This spectral reflectance difference is removed by normalizing the BRDF shapes by multiplying through a scale factor $K = \alpha/f_{iso}$ (Jiao, et al., 2012). Here, α is an adjustment factor to limit the range of the adjusted shapes and α is equal to 0.5 in this research to force most shapes into 0—1.0. The normalize process only transforms the isotropic parameters into the same level so that the BRDF of different land cover can be compared directly. However, anisotropic feature does not change during this process. Fig. 2 shows the principle plane BRDF shapes of three typical land covers. Gray lines represent the origin BRDF shape and dark line represents the BRDF shape after normalizing. The AFX value of the rough bail soil is 0.73, suggesting that geometrical optics scattering is greater than volume scattering, and the BRDF shape performs as a dome shape. The dense wheat has an AFX of 1.24 and volume scattering is greater than geometrical optics scattering. At this point, BRDF shape perform as a bowl shape. As to the flat salt land, the AFX is 1.01 and the BRDF shape is more smoother.

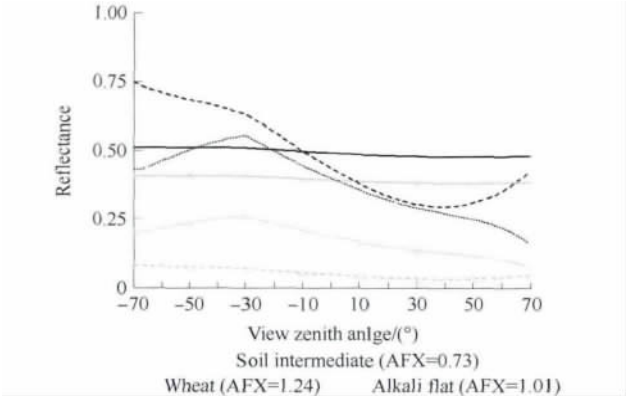

Fig. 2 BRDF shapes on principle for three typical land covers in the red band

2.2.3 Extract BRDF archetype from multi-angle datasets

The preceding analysis suggests that AFX has good ability in indicating the scattering form. Taking AFX as an indicator of BRDF character, we can establish a BRDF archetype (each BRDF shape represents non-repetition BRDF shape in a particular band, so the shape is called the BRDF archetype), which can present the change of BRDF and can help the application of BRDF as a priori knowledge. To extract BRDF archetype, the kernel driven BRDF model is used to fitting field observations first to get model parameters and AFX. Then Iterative Self Organizing Data Analysis Techniques Algorithm (ISODATA) method is used to classify the AFX, and the mean values of each class are used as BRDF archetype's parameters. Finally, the spectral normalizing is performed, and here we normalize the isotropic parameter to 0.5.

To determine the optimal number of the BRDF archetype, we classified those data sets into two to nine classes. We used each BRDF archetype fitting the data within the class, and calculated the fitting error of each data. Study shows that with the increase of the number of class, the mean value and standard deviation of the fitting error are gradually reduced. When the number of archetype is greater than four, there are no obvious changes in fitting error, which kept at 0.018 and 0.04 level in the red and near-infrared bands. Considering the complexity of the algorithm and the accuracy of the results, finally, the BRDF archetype database with four BRDF shapes is built in the two bands, respectively. More details about the establishing of BRDF types can refer to Jiao, et al. (2012). Table 1 lists the before (f) and after normalize (F) model parameters as well as the AFX values. The BRDF shape on the principle is shown in Fig. 3, and the left is red band and right is the nearinfrared band. The shapes from bottom to top are corresponding to R1 to R4 or N1 to N4, respectively. From Table 1 and Fig. 3, we can see that with the increase of AFX, the normalized volume scattering parameter gradually increased and geometrical scattering parameter gradually decreased, suggesting that the role of geometrical scattering gradually weakened while volume scattering effect gradually increased, and the BRDF shape transformed from dome shape to bowl shape.

Tablel 1 Model parameter and AFX value of each BRDF archetype

	Class	AFX_{mean}	f_{iso}	f_{vol}	f_{geo}	F_{iso}	F_{vol}	F_{geo}
Red bands	R1	0.6714	0.2040	0.0690	0.0552	0.5	0.1724	0.1429
	R2	0.8916	0.1341	0.0338	0.0160	0.5	0.1868	0.0650
	R3	1.0060	0.0899	0.0571	0.0079	0.5	0.3875	0.0511
	R4	1.2412	0.0391	0.0526	0.0010	0.5	0.7097	0.0099
Near infrared bands	N1	0.6855	0.3713	0.1023	0.0995	0.5	0.1508	0.1349
	N2	0.9202	0.2857	0.1021	0.0311	0.5	0.2048	0.0571
	N3	1.0460	0.3168	0.1855	0.0149	0.5	0.3097	0.0258
	N4	1.1808	0.3390	0.3261	0.0006	0.5	0.4881	0.0014

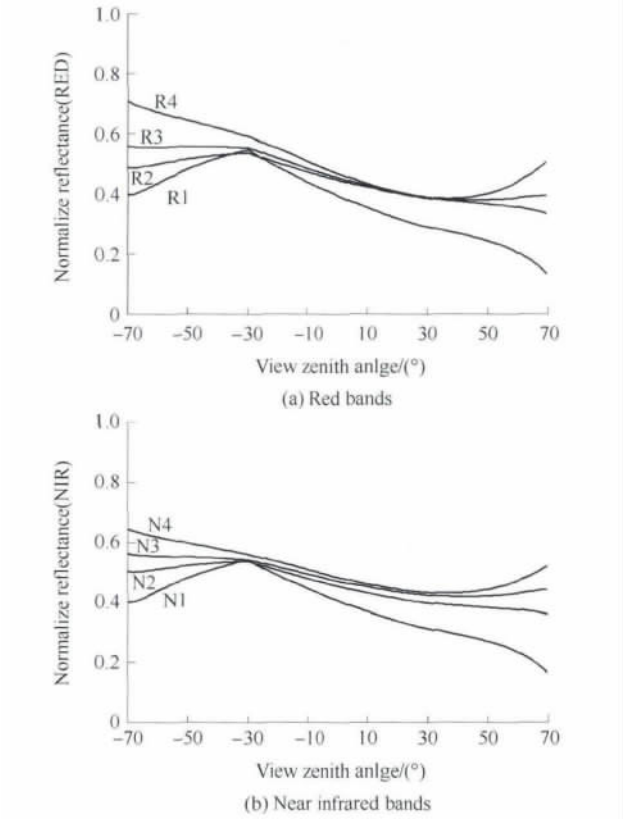

Fig. 3 BRDF archetype shapes on the principle plane in the red and near infrared bands at the 30° sun zenith angle

3 ARCHETYPE INVERSION METHOD AND VALIDATION

3.1 Archetype inversion

BRDF Archetype effectively summarizes the surface reflectance anisotropy and it can be used as a priori knowledge for the retrieval of albedo from multi-angle observations. Using those BRDF archetypes fitting the observations, respectively, the best BRDF archetype, which has the smallest RMSE, can be determined. This is the basic idea of the study. Consider a set of n BRF multi-angular measurements, $\boldsymbol{B}$: $\boldsymbol{B} = \rho_0(\boldsymbol{\Omega}_{i,0};\boldsymbol{\Omega}_{r,0}), \rho_1(\boldsymbol{\Omega}_{i,1};\boldsymbol{\Omega}_{r,1}), \cdots, \rho_{n-1}(\boldsymbol{\Omega}_{i,n-1};\boldsymbol{\Omega}_{r,n-1})$. The archetypical BRDF of the observation is assumed as BRDF′. BRFs from archetypical BRDF can be retrieved through the RTLSR model in the forward model, $\boldsymbol{B}'$: $\boldsymbol{B}' = \rho_0'(\boldsymbol{\Omega}_{i,0};\boldsymbol{\Omega}_{r,0}), \rho_1'(\boldsymbol{\Omega}_{i,1};\boldsymbol{\Omega}_{r,1}), \cdots, \rho_{n-1}'(\boldsymbol{\Omega}_{i,n-1};\boldsymbol{\Omega}_{r,n-1})$. We then find the adjustment value a that minimizes the difference between $\boldsymbol{B}$ and $a\boldsymbol{B}'$ using the technical of least-mean squares. We minimized an error term e^2 given by (Strugnell & Lucht, 2001):

$$e^2 = \sum_{i=0}^{n-1}(\rho_i - a\rho_i')^2 \tag{4}$$

it follows that

$$a = \frac{\sum_{j=0}^{n-1}\rho_j \times \rho_j'}{\sum_{j=0}^{n-1}(\rho_j')^2} \tag{5}$$

then, the BRDF can be calculated

$$\text{BRDF} = a \times \text{BRDF} \tag{6}$$

and the fitting error can be write as

$$\text{RMSE} = \sqrt{\frac{1}{n-1}\sum_{k=0}^{n-1}(\rho_k - a\rho_k')^2} \tag{7}$$

Using those four BRDF archetypes fitting the observations, respectively, RMSE of each BRDF archetype can be calculated and the BRDF arcehtype which has the smallest RMSE was s elected as a priori knowledge of the data. Through the Eq. (5), the adjustment a can be calculated. BSA and WSA of the data can be computed from prior BSA′ and WSA′:

$$\text{BSA}(\theta,\lambda) = a \times \text{BSA}'(\theta,\lambda) = a \times \sum_k F_k(\lambda)h_k(\theta) \tag{8}$$

$$\text{WSA}(\lambda) = a \times \text{WSA}'(\lambda) = a \times \sum_k (F_k(\lambda)H_k) \tag{9}$$

where $h_k(\theta)$ and H_k are the directional-hemispherical and bi-hemispherical integrals of the BRDF model kernels, and they do not depend on the observations and may be pre-computed and stored. Constant 0.189184 and 1.377622 are the bi-hemispherical integral of the RossThick kernel and reciprocal LiSparse kernel.

3.2 Method validation

The surface reflectance anisotropic character is more obvious on the principle plane while it performed smooth on the cross-principle plane (Li & Strahler, 1992). From Fig. 2 and Fig. 3 we also can see, when the AFX value is large or small than a u nit, the reflectance on the principle plane will change obviously with view zenith angle. There is a "hot spot" in the back forward direction, and a "dark spot" in the forward direction. The reflectance also changed largely at large view zenith angles. Moreover, the effect of surface reflectance anisotropic on reflectivity also connects to the amount of the spectrum. In Fig. 2, the wheat has an AFX of 1.24, and has more volume scattering b ehavior, but its spectrum level only ranged from 0.05 to 0.1. After the

normalizing, the reflectance varied from 0.3 to 0.75, indicating that when the reflectance anisotropic is similar, the large the spectrum, the more diversity will be caused by the reflectance anisotropic. Seeing from the different direction on the cross-principle plane, the proportion of the shadow area is relatively stable, so the BRDF shape is relatively smooth and there is no dramatic changes.

To evaluate the accuracy of our algorithm, the observations in each datasets that have a view zenith angle less than 40° and distribute on the principle, cross-principle, 30° or 60° plane are selected as new validation data sets. Both the full inversion method and archetype method were used to fitting the validation data. The results are compared with the standard result, which is retried from the full inversion method and all observations. The number of observations of each validation data ranged from 4 to 12. All of those observations in one data have the similar sun zenith angle. The observation datasets are obtained under several sun zenith angles, so more than one validation dataset may be yield from one observation datasets. Those validation data meet the MODIS back up requirement (Jin, et al., 2013), and can represent the observations that lack of sampling information.

Comparing the WSA from the validation data sets using archetype inversion and full inversion method with the standard value, the scatter plots are shown in Fig. 4, and the accuracy of result are given in Table 2. Compared results showed that: (1) When the observations are not on the cross principle plane, the lowest coefficient of determination between standard value and WSA from archetype inversion is 0.944 in the red band, while the highest coefficient of determination between standard value and WSA from full inversion is 0.927. The largest relative errors of those two methods are 17.14% and 27.63% obtained in 60 degree plane. The archetype method can improve the results by about 5%—10%. The near-infrared band has a similar result and it has a 3%—8% improvement. (2) When the observations are on the cross-principle plane, the coefficient of determination of the two bands between standard value and WSA from archetype method is 0.36, and the largest relative error is as high as to 0.18. However, the results of archetype inversion are more credible, and the largest absolute and relative errors are 0.037 and 13.52%, respectively. (3) The full inversion method failed (albedo greater than 1 or less than 0) for 17 and 26 validation datasets in red and near-infrared bands. Open circle and triangle in Fig. 4 represent the data sets that failed or the absolute error with the standard value greater than 0.1. However, results of archetype inversion method are all acceptable. To sum up, under the condition of insufficient of multi-angular observations information, the accuracy of archetype information is higher than full inversion method, and this behavior is more obvious when the observations are on the cross-principle plane.

The full inversion method relied on kernel driven model and has a strict limit on the distribution of sampling and the noise in observations (Jin, et al., 2003; Shuai, et al., 2008). Archetype inversion method, which is based on the full inversion method, can restrict BRDF in whole space using a priori knowledge. The validation data sets used in this study have the sun zenith angle less than 40°, and they lack observations in large view zenith angles. When the selected observations are on the principle plane, they can represent the surface reflectance anisotropic on some degree. However, the anisotropic on cross-principle plane is limited, so the observations on this plane are not that representative. So, when observations locate on the principle plane, full inversion and archetype inversion methods can get better results, and archetype inversion method performed even better. With the sampling plane moving away from the principle plane (from principle plane to 30°, 60°, and cross-principle plane), the accuracy of full inversion dropped obviously and even failed, but the accuracy of archetype inversion method kept stable. It shows that the archetype inversion method can be used to ill-posed data sets and can get stable results. It should be noted that, on the 60 degree plane, the archetype inversion accuracy is slight lower, and this may be caused by the representation of the observations and also may be decided by the number of the data sets. There are only 57 data sets are used in this group and other three groups had more than 100 sets. Generally, multi-angle observations like the validation data in this study may not have enough directional information, but the archetype inversion method, which using BRDF archetype as a priori knowledge, can describe anisotropic and albedo more accurately. This advantage is more significant when the date has a poor sampling.

In order to explain the advantage of archetype inversion method in poor sampling data sets more clearly, we selected four data sets, which had observations located on different planes for analysis. The observations and BRDF shapes of the four data sets on the principle plane with different methods are shown in Fig. 5. Table 3 shows the results of WSA and the absolute error with the standard value. It can be seen that when the observations can represent part of the surface anisotropy, both of the method can get an accurate result (Fig. 5(a)). Due to the poor sampling and noise in observations, archetype inversion performed a little better than full inversion. However, when there are obvious noises and lack observations on the hot spot, full inversion method will become less stable (Fig. 5(b)). When the observations are on the cross-principle, observations are not representative and there are no observations in the large zenith angle, and the results will become unreliable and even fail (Fig. 5(a)(b)). Archetype inversion method introduce a priori knowledge and constraint the BRDF in the entire spatial. This method has a weak dependence on the observation samples and good at undermining the noise, and thus, can retrieve accurate albedo. At present, a large number of sensors' multi-angle sampling ability is limited and the archetype inversion method may have a broad application prospects.

Table 2 The accuracy of archetype inversion method

Bands	Plane	RMSE1	RMSE2	ε_1/%	ε_2/%
Red	PP	0.02325	0.01217	21.630	11.906
	30P	0.02272	0.01834	17.483	12.681
	60P	0.02382	0.01862	27.631	17.135
	CP	0.18281	0.02173	99.306	13.515
Nir	PP	0.04667	0.03325	13.791	9.440
	30P	0.05007	0.03555	13.287	10.227
	60P	0.05733	0.03100	18.574	10.872
	CP	0.18469	0.03692	46.921	9.760

Note: RMSE1, RMSE1, ε_1 and RMSE2, ε_2 represent the absolute error and the relative error between full inversion result or archetype inversion results and standard results. PP, 30P 60p, and CP are represent principle plane, 30°, 60° and cross-principle plane.

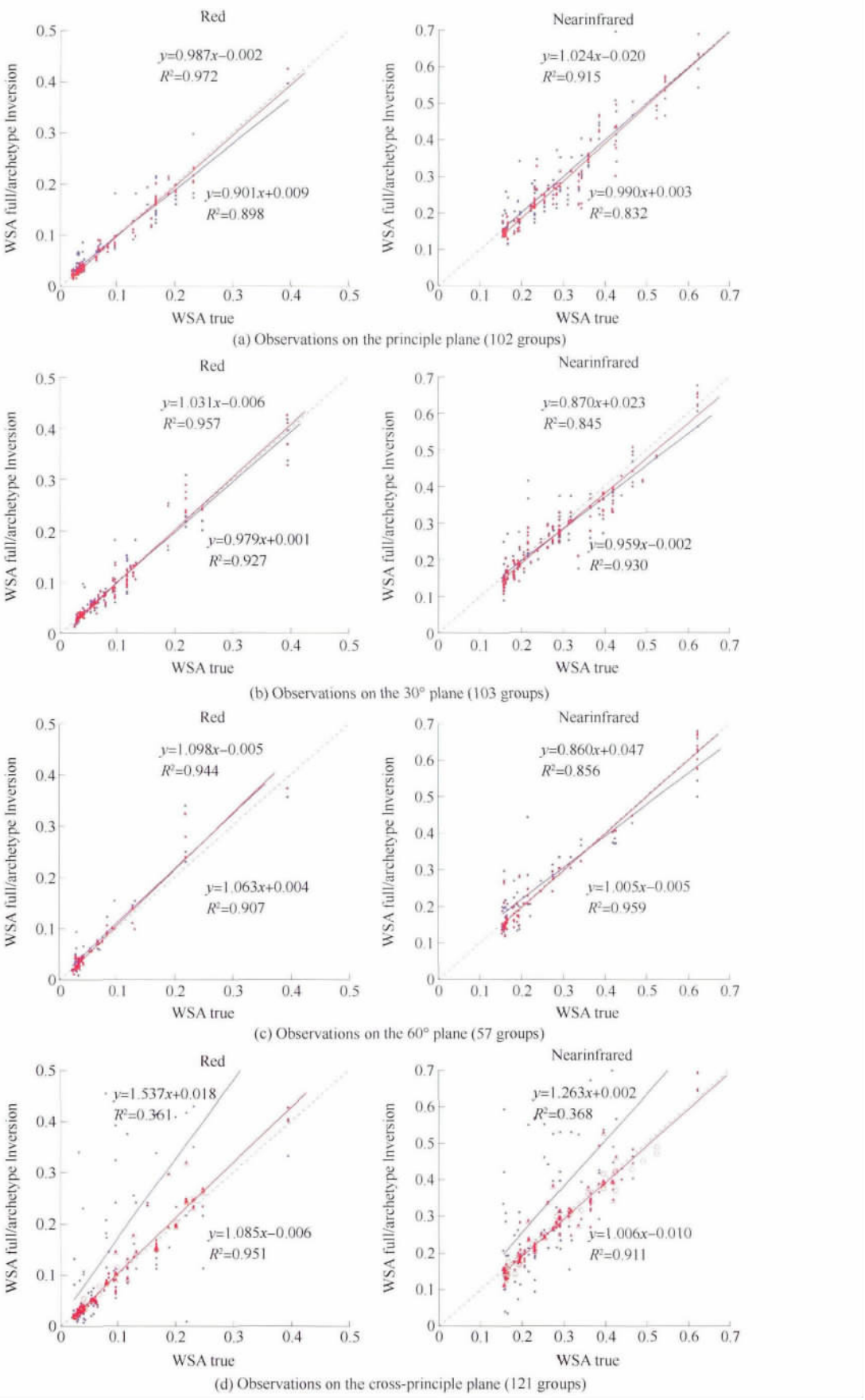

Fig. 4 Scatter plot of WSA from the validation data using full inversion and archetype inversion methods vs. standard WSA. (The red and blue color represents archetype inversion and full inversion results. Open circle and triangle represent data sets that failed or absolute error is greater than 0.1)

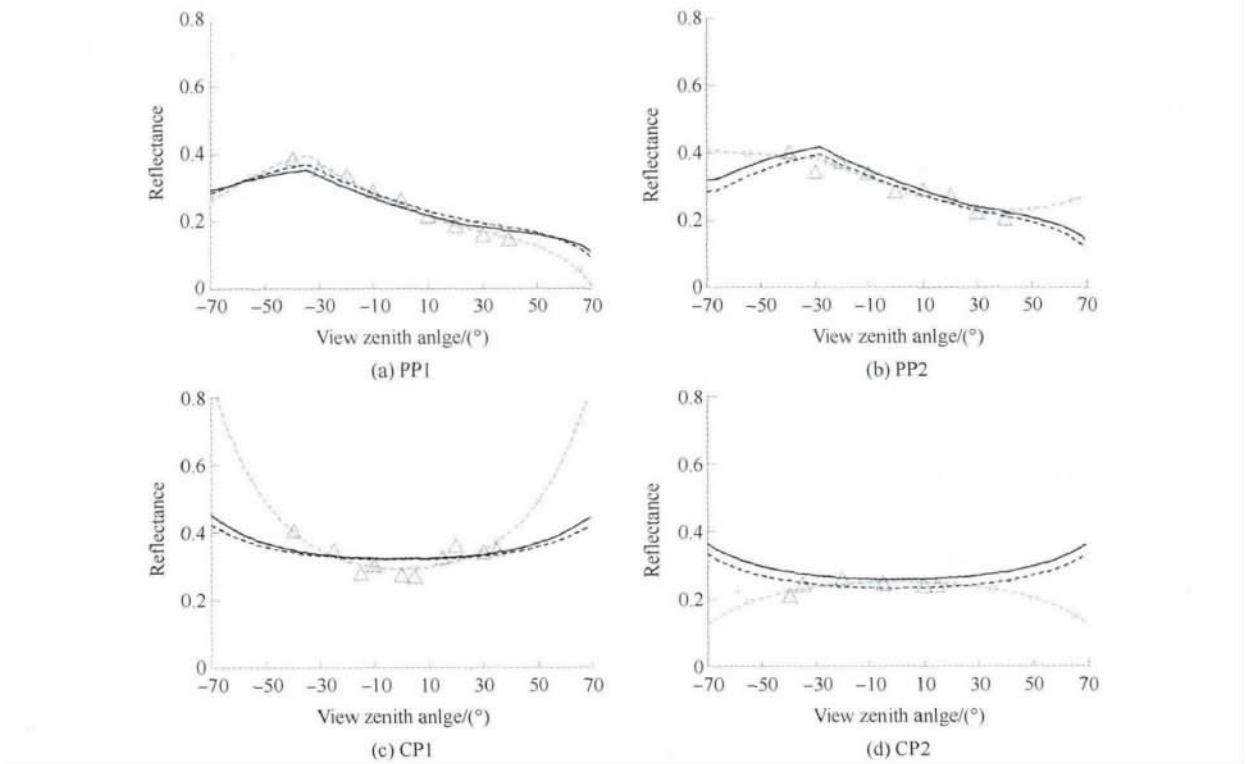

Fig. 5 The distribution of observation and BRDF shape on the principle plane
(The dark line is the standard BRDF shape, the dark dot line is the shape of archetype inversion method, and gray dot line respresents the full inversion result. Triangles are the observations, PP is principle, CP is cross principle plane)

Table 3 White sky albedo and inversion accuracy of validation datasets in Fig. 5

	WSA_T	WSA_F	WSA_A	D_{ft}	D_{at}
PP1	0.23157	0.19388	0.22671	0.0377	0.0049
PP2	0.28360	0.37039	0.25294	0.0868	0.0307
CP1	0.41742	0.70213	0.39599	0.2847	0.0214
CP2	0.29094	0.21124	0.27212	0.0797	0.0188

Note: WSA_T is the standard vaule of WSA. WSA_F is full inversion result. WSA_A is archetype inversion result. D_{ft}, D_{at} represent the absolute error between WSA_A and WSA_F and between WSA_T and WSA_F.

4 CONCLUSION

This study built BRDF archetype database according to field multi-angular data sets and AFX which can indicate the s urface reflectance anisotropy. We outlined an algorithm for the derivation of land surface albedo from poor sampling multi-a ngular observations and explored the potential accuracy of such a technique using simulate validation data sets. This study p rovided a new way for the application of a priori knowledge and has a great significant role for those ill posed multi-angle data sets. The conclusions are as below.

(1) AFX has the ability to indicate the variance of BRDF, and with the increase of AFX, the volume scattering effect gradually increased and geometric scattering effect gradually weakened. The archetype, which is established from field observations and AFX, can effectively summarize the surface reflectance a nisotropy. It provides a new way for the extract and use of a priori knowledge.

(2) A priori knowledge can effectively solve the problem of insufficient number of observation in remote sensing. The advantage of the archetype inversion method is that it is able to c onstraint the BRDF in the whole spatial space and use the maximum information of the observations. Thus, this method can get albedo even for the data that has ill posed problem.

(3) Comparing the archetype method with the full inversion method, when there is limited number of observations and has ill posed problems, the former has much higher accuracy and more stable results. It is independent on the number of the observations, the distribution of the view and the quality of the observations. Generally, for the ill posed data, archetype inversion method can advance the accuracy by up to 3%—10%, especially for the data sets that have their observations on the cross-principle plane.

The field multi-angle data sets used in this study were mainly obtained in dormancy seasons, and this may ignore the effect of seasons. To acquire more typically BRDF archetypes, the observation database should be expanded and recruited. In future, we will add POLDER datasets and MODIS BRDF product on EOS core sites to renew the BRDF archetype. Moreover, we will analyze the application conditions, including the effect of the variance of seasons, the correlation of the BRDF a rchetype between different bands.

REFERENCES

Bacour C and Bréon F M. 2005. Variability of biome reflectance directional signatures as seen by POLDER. Remote Sensing of Environ-

ment, 98(1): 80 – 95 [DOI: 10.1016/j.rse.2005.06.008]

Dickinson R E. 1983. Land surface processes and climate surface albedos and energy balance. Advances in Geophysics, 25: 305 – 353 [DOI: 10.1016/S0065 – 2687(08)60176 – 4]

Deering D W and Leone P. 1986. A sphere-scanning radiometer for rapid directional measurements of sky and ground radiance. Remote Sensing of Environment, 19(1): 1 – 24 [DOI: 10.1016/0034 – 4257(86)90038 – 6]

Deering D W, Eck T F and Grier T. 1992. Shinnery oak bidirectional reflectance properties and canopy model inversion. IEEE Transactions on Geoscience and Remote Sensing, 30(2): 339 – 348 [DOI: 10.1109/36.134083]

Dickinson R E. 1995. Land processes in climate models. Remote Sensing of Environment, 51(1): 27 – 38 [DOI: 10.1016/0034 – 4257(94)00062 – R]

Deering D W, Eck T F and Banerjee B. 1999. Characterization of the reflectance anisotropy of three boreal forest canopies in spring-summer. Remote Sensing of Environment, 67(2): 205 – 229 [DOI: 10.1016/S0034 – 4257(98)00087 – X]

Hu B X, Lucht W, Li X W and Strahler A H. 1997. Validation of kernel-drives semiempirical models for the surface bidirectional reflectance distribution function of land surfaces. Remote Sensing of Environment, 62(3): 201 – 214

Huang X, Jiao Z, Dong Y, Zhang H and Li X. 2013. Analysis of BRDF and albedo retrieved by kernel-driven models using field measurements. IEEE Journal of Selected Topics in Applied Earth Observations and Remote Sensing, 6(1): 149 – 161 [DOI: 10.1109/JSTARS.2012.2208264]

Irons J R, Campbell G S, Norman J M, Graham D W and Kovalick W M. 1992. Prediction and measurement of soil bidirectional reflectance. IEEE Transactions on Geoscience and Remote Sensing, 30(2): 249 – 260 [DOI: 10.1109/36.134075]

Jiao Z T, Li X W, Wang J D and Zhang H. 2011. Assessment of MODIS BRDF shape indicators. Journal of Remote Sensing, 15(3): 432 – 456

Jiao Z, Zhang H and Li X W. 2012. To derive a prior database of archetypal BRDF shapes from ground measurements using anisotropic flat index (AFX) // Proceedings of the IEEE International Geoscience and Remote Sensing Symposium (IGARSS). Munich: IEEE: 6753 – 6756 [DOI: 10.1109/IGARSS.2012.6352555]

Jin Y F, Schaaf C B, Woodcock C E, Gao F, Li X W, Strahler A H, Lucht W and Liang S. 2003. Consistency of MODIS surface bidirectional reflectance distribution function and albedo retrievals: 1. Algorithm performance. Journal of Geophysical Research-Atmospheres, 108(D5): 4158 [DOI: 10.1029/2002JD002803]

Kimes D S. 1983. Dynamics of directional reflectance factor distributions for vegetation canopies. Applied Optics, 22(9): 1364 – 1372 [DOI: 10.1364/AO.22.001364]

Kimes D S, Newcomb W W, Nelson R F and Schutt J B. 1986. Directional reflectance distributions of a hardwood and pine forest canopy. IEEE Transactions on Geoscience and Remote Sensing, G E – 24(2): 281 – 293

Leroy M and Breon F M. 1996. Angular signatures of surface reflectances from airborne POLDER data. Remote Sensing of Environment, 57(2): 97 – 107 [DOI: 10.1016/0034 – 4257(95)00229 – 4]

Lewis P and Barnsley M J. 1994. Influence of the sky radiance distribution on various formulations of the earth surface albedo // Proc. Conf. Phys. Meas. Sign. Remote Sens., Val d'Isere, France: 707 – 715

Li X and Strahler A H. 1992. Geometric-optical bidirectional reflectance modeling of the discrete crown vegetation canopy: effect of crown shape and mutual shadowing. IEEE Transactions on Geoscience and Remote Sensing, 30(2): 276 – 292 [DOI: 10.1109/36.134078]

Li X W and Wang J D. 1995. Vegetation Optical Remote Sensing Model and Vegetation Structure Paramerization. Beijing: Science Press

Li X and Strahler A H. 1985. Geometric-optical modeling of a conifer forest canopy. IEEE Transactions on Geoscience and Remote Sensing, GE-23(5): 705 – 721 [DOI: 10.1109/TGRS.1985.289389]

Li X W, Gao F, Wang J D and Strahler A. 2001. A priori knowledge accumulation and its application to linear BRDF model inversion. Journal of Geophysical Research: Atmospheres, 106(D11): 11925 – 11935 [DOI: 10.1029/2000JD900639]

Liu J, Schaaf C, Strahler A, Jiao Z T, Shuai Y, Zhang Q L, Roman M, Augustine J A and Dutton E G. 2009. Validation of Moderate Resolution Imaging Spectroradiometer (MODIS) albedo retrieval algorithm: Dependence of albedo on solar zenith angle. Journal Geophysical Reserarch, 114 (D1): D01106 [DOI: 10.1029/2008JD009969]

Lucht W, Schaaf C B and Strahler A H. 2000. An algorithm for the retrieval of albedo from space using semiempirical BRDF models. IEEE Transactions on Geoscience and Remote Sensing, 38(2): 977 – 998 [DOI: 10.1109/36.841980]

Nicodemus F E, Richmond J C, Hsia J J, Ginsberg I W and Limperis T. 1977. Geometrical Considerations and Nomenclature for Reflectance. Washington, DC: National Bureau of Standards, US Department of Commerce

Ranson K J, Biehl L L and Bauer M E. 1985. Variation in spectral response of soybeans with respect to illumination, view and canopy geometry. International Journal of Remote Sensing, 6(12): 1827 – 1842 [DOI:10.1080/01431168508948331]

Roman M O Gatebe C K, Schaaf C B, Poudyal R, Wang Z S and King M D. 2011. Variability in surface BRDF at different spatial scales (30 m—500 m) over a mixed agricultural landscape as retrieved from airborne and satellite spectral measurements. Remote Sensing of Environment, 115(9): 2184 – 2203 [DOI: 10.1016/j.rse.2011.04.012]

Roujean J L, Leroy M and Deschamps P Y. 1992. A bidirectional reflectance model of the Earth's surface for the correction of remote sensing data. Journal of Geophysical Research, 97(D18): 20455 – 20468 [DOI: 10.1029/92JD01411]

Schaaf C B, Gao G, Strahler A H, Lucht W, Li X, Tsang T, Strugnell N C, Zhang X, Jin Y, Muller J P, Lewis P, Barnsely M J, Hobson P, Disney M, Roberts G, Dunderdale M, Doll C, D'Entremont R P, Hu B, Liang S, Privette J and Roy D P. 2002. First operational BRDF, albedo nadir reflectance products from MODIS. Remote Sensing of Environment, 83(1/2): 135 – 148 [DOI: 10.1016/S0034 – 4257(02)00083 – 4]

Shuai Y, Schaaf C B, Strahler A H, Liu J and Jiao Z. 2008. Quality assessment of BRDF/albedo retrievals in MODIS operational system. Geophysical Research Letters, 35 (5) [DOI: 10.1029/2007GL032568]

Strahler A H and Jupp D L B. 1990. Bidirectional reflectance modeling of forest canopies using boolean models and geometric optics // Proceedings of Remote Sensing Science for the Nineties', 10th Annual International. Geoscience and Remote Sensing Symposium. USA: IEEE: 1751 – 1755 [DOI: 10.1109/IGARSS.1990.688854]

Strugnell N C and Lucht W. 2001. An algorithm to infer continental-scale albedo from AVHRR data, land cover class, and field observations of typical BRDFs. Journal of Climate, 14(7): 1360 – 1376 [DOI: 10.1175/1520 – 0442(2001)014 < 1360:AATICS > 2.0.CO;2]

Tsay S C, King M D, Arnold G T and Li J Y. 1998. Airborne spectral measurements of surface anisotropy during SCAR-B. Journal of Geophysical Research-Atmospheres, 103(D24): 31943 – 31953

Vierling L A, Deering D W and Eck T F. 1997. Differences in arctic tundra vegetation type and phenology as seen using bidirectional radiometry in the early growing season. Remote Sensing of Environment, 60(1): 71 – 82 [DOI: 10.1016/S0034 – 4257(96)00139 – 3]

Wanner W, Li X and Strahler A H. 1995. On the derivation of kernels for kernel-driven models of bidirectional reflectance. Journal of Geophysical Research, 100(D10): 21077 – 21089 [DOI: 10.1029/95JD02371]

基于 BRDF 原型反演地表反照率

张虎，焦子锑，董亚冬，黄兴英，李佳悦，李小文

1. 北京师范大学 地理学与遥感科学学院，北京 100875；
2. 遥感科学国家重点实验室 北京师范大学，北京 100875；
3. 北京师范大学 环境遥感与数字城市北京市重点实验室，北京 100875

摘　要：先验知识在遥感反演中起到重要的作用，本文首先根据各向异性平整指数 AFX 和地表多角度观测数据集建立了 BRDF 二向性反射分布函数原型库，然后介绍了以 BRDF 原型作为先验知识的提取多角度数据地表反照率的原型反演算法，为验证算法的精度，将原型反演及全反演算法拟合验证数据子集得到的反照率与 MODIS 全反演算法拟合完整数据集得到的结果作比较。结果对比表明，观测天顶角在 40°以内时，非垂直主平面的观测数据能够代表部分地表的各向异性反射特征，此时原型反演算法的最大平均绝对误差为 0.036，相对精度比全反演算法高约 5%—10%；当数据位于垂直主平面时，观测信息量严重不足，此时原型反演算法结果相对较稳定，而全反演算法的最大绝对误差高达 0.18。综上所述，原型反演算法能够在整个采样空间范围内对 BRDF 进行约束，对观测数据位置分布的依赖较小，抗噪声能力强，在反演观测信息不足的多角度数据时，结果精度优于全反演算法。

关键词：各向异性平整指数 AFX，BRDF 原型，原型反演，MODIS 全反演，反照率

中图分类号：TP701　　**文献标志码**：A

引用格式：张虎，焦子锑，董亚冬，黄兴英，李佳悦，李小文. 2013. 基于 BRDF 原型反演地表反照率. 遥感学报，17(6)：0000－0000

Zhang H，Jiao Z T，Dong Y D，Huang X Y，Li J Y and Li X W. 2013. An algorithm for retrieval albedo from BRDF archetype. Journal of Remote Sensing，17(6)：0000－0000　[DOI：10.11834/jrs.20133022]

1　引　言

自然条件下地表的反射是各向异性的，通常由二向性反射分布函数 BRDF（Nicodemus 等，1977）来描述，BRDF 在空间范围内的积分得到地表反照率。反照率定义为整个太阳光谱范围内陆地表面向各个方向反射的太阳辐射能与总入射的太阳辐射能的比（Dickinson，1983），它反映了地面对太阳辐射的反射能力，是监测地表能量交换的重要参数，也是气候模型的一个基本参数，在地表能量平衡和全球气候变化的研究中发挥重要作用（Dickinson，1995）。因此，获取高精度的地表反照率，对研究区域气候变化以及改进和验证陆面过程模型具有重要意义。

从地表方向反射率定量估算地表反照率及植被和土壤特征需要考虑地表的各向异性特征（李小文和王锦地，1995）。目前，地表反射的各向异性校正及多角度数据地表反照率反演，多是通过核驱动模型对多角度的观测数据进行拟合，然后通过核的外推和积分来完成（Lucht 等，2000；Schaaf 等，2002；Strugnell 和 Lucht，2001）。然而，受传感器采样能力的限制以及云的影响，遥感多角度数据（如 MODIS）通常是假定地物在一定时期内地表的各向异性特征保持不变，通过长时间的积累观测，实现对地物的多角度观测（Jin 等，2003；Schaaf 等，2002）。然而影响地物方向反射的因素众多，太阳天顶角、气象条件及下垫面状况的改变都会引起方向反射率较大的差异（Liu 等，2009；Strugnell 和 Lucht，2001）。对于高分辨率数据，受传感器采样能力的约束更为显著，通常仅能获得某一个特定方向的观测数据，很难在短时间内获得大区域范围的多角度数据。此外，核驱

收稿日期：2013-01-28；修订日期：2013-05-27；优先数字出版日期：2013-06-03

基金项目：国家高技术研究发展计划（863 计划）（编号：2012AA12A304）；国家自然科学基金（编号：41171261，40871193）

第一作者简介：张虎（1986—　），男，博士研究生，研究方向为定量遥感、地表二向性反射以及地表反照率的应用研究。E-mail：askzhanghu@126.com

通信作者简介：焦子锑（1970—　），男，博士，副教授，现从事定量遥感、地表各向异性反射的建模与应用，以及多角度信号用于地表分类的研究等，已发表论文 20 余篇。E-mail：jiaozt@bnu.edu.cn

动模型反演地表反照率算法对观测的数量及观测角度分布都有较高的要求(Jin 等,2003),这些因素都限制了地表反照率的反演精度。

先验知识能够有效地解决遥感反演中信息量不足的问题。在现有的基于先验 BRDF 形状的算法中,通常假定同一种地表类型有相似的 BRDF 形状,通过先验的形状拟合少数几个观测,得到拟合观测数据较优的 BRDF 形状(Strugnell 和 Lucht,2001)。但也有研究表明,对于多数地类 BRDF 形状在类内的方差大于类间的方差(Bacour 和 Bréon,2005),这主要是因为 BRDF 与地物的空间结构特征密切相关(Li 和 Strahler,1985;Li 和 Strahler,1992;Strahler 和 Jupp,1990),不同地表类型可能表现出相似的空间结构特征。同时,BRDF 还受到尺度效应的影响,研究表明当像元尺度在千米级以上时,其空间异质性较小,这种情况下通常认为不同地类的 BRDF 形状相近(Bacour 和 Bréon,2005),随着像元尺度的减小,空间异质性特征逐渐显著,BRDF 形状会随着下垫面植被空间结构的变化而出现有明显的差异(Roman 等,2011)。

本研究借助半经验核驱动的 BRDF 模型(Ross-Thick-LiSpareR)(Wanner 等,1995)对地表观测数据集进行拟合,通过模型参数计算得到各向异性平整指数(AFX)(焦子锑等,2011),根据 AFX 对地表各向异性反射的指示作用,首先建立了地表 BRDF 原型库,然后提出了以 BRDF 原型作为先验知识,在多角度数据空间采样不足时,估算地表反照率的 BRDF 原型反演算法,最后用验证数据对比研究了 MODIS 全反演算法(Lucht 等,2000)和原型反演算法结果的精度差异,并对造成差异的原因进行了分析。

2 数据和理论基础

2.1 多角度观测数据

地面多角度测量的主要优势在于能够在短时间内实现对同一地物不同方向的观测,有利于地表各向异性特征的研究。本文中应用的 73 组多角度数据集的下垫面地表类型包括土壤、稀疏草地、灌木丛、阔叶作物和森林等。其中大部分为地面多角度观测数据(Kimes 等,1983,1986;Ranson 等,1985;Deering 等,1992,1986,1999;Irons 等,1992;Vierling 等,1997),此外还有机载的 POLDER 数据(Leroy 和 Breon,1996)和 CAR 数据(Tsay 等,1998)等,Huang 等人(2013)给出了每一组数据的具体信息。这些数据只有红和近红外两个波段,大部分数据曾被用于验证半经验的核驱动模型的拟合能力以及算法的研究(Li 等,2001;Hu 等,1997),具有很好的代表性。

2.2 理论基础

2.2.1 核驱动模型

地物的反射通常是各向异性的,地表的方向反射率可以根据太阳和观测角度的函数来描述。核驱动模型常用来从多角度观测数据反演地表反照率,它是用一定物理意义的核的线性组合来描述地表的二向性反射特征,即对于地表的一个非朗伯像元,其表面散射可以表示为各向同性散射,体散射和几何光学散射 3 种组分的加权和的形式(Lucht 等,2000;Roujean 等,1992;Wanner 等,1995):

$$R(\theta_i,\theta_r,\varphi) = f_{\text{iso}}(\lambda) + f_{\text{vol}}(\lambda)K_{\text{vol}}(\theta_i,\theta_r,\varphi) + f_{\text{geo}}(\lambda)K_{\text{geo}}(\theta_i,\theta_r,\varphi) \quad (1)$$

式中,R 为太阳天顶角 θ_i、观测天顶角 θ_r 和相对方位角 φ 处的方向反射率;K_{vol} 为体散射核,K_{geo} 为几何光学核,它们都是入射角和观测角的函数,在 R 中所占的比例通过 f_{geo} 和 f_{vol} 来权衡,f_{iso} 用来表示各向同性散射在 R 中的贡献。

MODIS 全反演算法通过线性回归,反演出拟合观测数据最优的 f_{iso}、f_{vol} 和 f_{geo},因为在拟合过程中体散射或几何光学散射核系数可能为没有物理意义的负值,我们将负系数强制设定为零,然后仅根据另外两个核反演得到核系数(Jin 等,2003)。核与待反演的参数无关,核的积分可以预先求出,将核的积分以 f_{iso}、f_{vol} 和 f_{geo} 为权重相加,就得到相应的黑天空反照率 BSA 和白天空反照率 WSA(Lucht 等,2000)。将黑天空和白天空反照率以散射光在总的入射光中所占的比例为权重相加,就得到了真实地表反照率(Lewis 和 Barnsley,1994)。大量验证表明,当多角度数据能够代表地表的各向异性特征时,全反演算法的结果和地表观测数据有很好的一致性(Jin 等,2003;Liu 等,2009;Schaaf 等,2002)。

文中选用的核分别为罗斯厚核(RossThick)和李氏稀疏互易核(LiSparseR)(Wanner 等,1995),它们在不同太阳天顶角时主平面的形状如图 1 所示,分别是一个典型的在大的观测天顶角反射率增强,略为前倾的“碗状”和一个在后向散射方向上,尤其在热点方向上,表现为峰值的“屋顶状”。实际的 BRDF 形状是这两种形状加权后的结果,所以通过核驱动模型得到的真实地面的 BRDF 形状也会呈现不同程度的“屋顶状”或是“碗状”的特征。

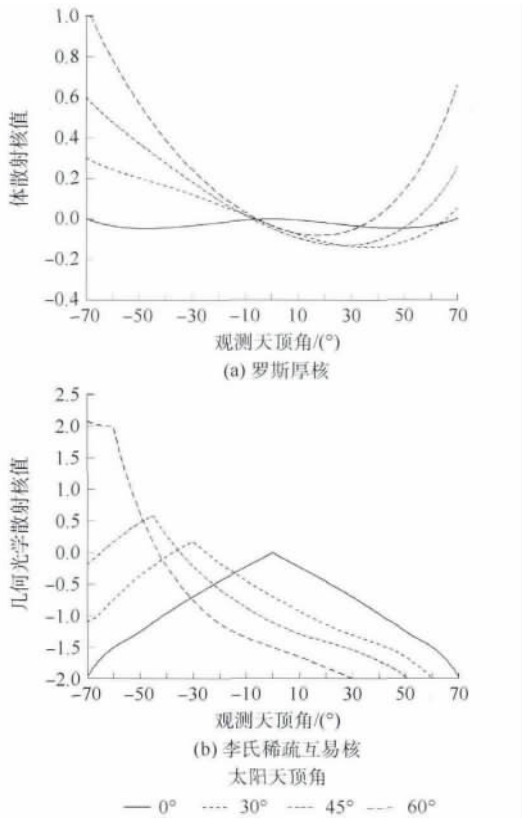

图 1 罗斯厚核与李氏稀疏互易核在不同太阳天顶角下主平面上的形状
(横坐标正值表示前向反射,负值表示后向反射)

2.2.2 各向异性平整指数

AFX 是根据核驱动模型的构造特点,针对 MODIS传感器的各向异性反射模式而构造的角度指数,定义为白天空反照率和地表各向同性参数 f_{iso} 的比 (焦子锑 等,2011):

$$\mathrm{AFX} = \frac{\mathrm{WSA}(\Lambda)}{f_{iso}(\Lambda)} \tag{2}$$

AFX 的大小依赖于波段 Λ,我们从核驱动模型公式出发,推导了 AFX 的另一种表达形式,可以把 AFX 与模型参数进行较好地结合,从而直接通过模型参数求出 AFX 值:

$$\mathrm{AFX} = 1 + \frac{f_{vol}(\Lambda)}{f_{iso}(\Lambda)} \times 0.189184 - \frac{f_{geo}(\Lambda)}{f_{iso}(\Lambda)} \times 1.377622 \tag{3}$$

式中,系数 0.189184 和 -1.377622 分别是对罗斯表层核和李氏稀疏互易核的双半球的积分值。

从式(3)可以看出,AFX 是被各向同性参数归一化的几何光学权重参数和体散射权重参数与两个核的积分的线性表达式。AFX 的大小依赖于几何光学和体散射这两个参数的大小,当体散射效应大于几何光学效应时,AFX > 1;当几何光学效应大于体散射效应时,AFX < 1;当两种效应很接近时,AFX ≈1。

地物反射率的大小与波段密切相关,裸地是典型的土壤背景地类,在红和近外波段的反射率水平相近;对于茂密的植被,由于受到叶绿素的影响,在红和近红外的反射水平差异较大;草地及灌木等稀疏植被反射率水平介于上述两种情况之间。通过观测数据拟合得到的 BRDF 形状(图 2 中灰线),将地表的各向异性特征与地物的光谱信息杂糅在一起,不便于研究。为消除光谱量的影响作用,提取纯 BRDF 效应,需要对各数据进行光谱归一化处理(Jiao 等,2012)。本研究中将各向同性参数 f_{iso} 归一成 0.5,即,$f_*' = 0.5 \times f_* / f_{iso}$。光谱归一化的作用是将各 BRDF 归一化到相同的数量级,便于不同地物 BRDF 间的对比,归一化过程中 AFX 大小并没有改变,即没有改变其相应的各向异性特征。如图 2 所示,灰线表示红波段主平面上地物真实的 BRDF 形状,受地表光谱量差异的影响,地物的各向异性特征无法直接进行比较;黑线表示光谱归一化之后的 BRDF 形状,对于粗糙的裸土,AFX 值为 0.73,即几何光学作用大于体散射作用,BRDF 呈现明显“屋顶状”,致密的小麦地 AFX 的值为 1.24,即几何光学作用小于体散射作用,BRDF 呈现“碗状”,而平坦的盐碱地两种散射作用相当,AFX 等于 1.01,BRDF 较平整。

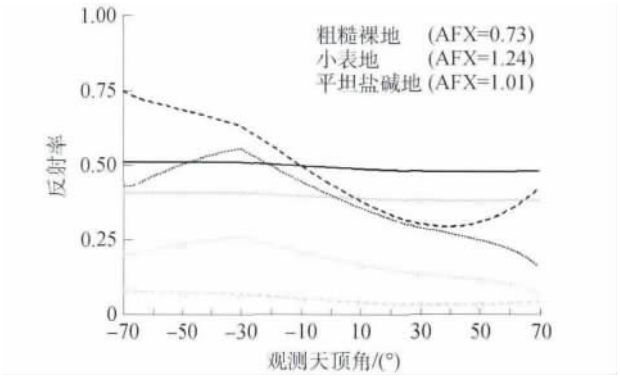

图 2 3 种典型在主平面上的 BRDF 形状及相应的 AFX 值
(灰色和黑色分别为归一化前和后红波段地物的形状)

2.2.3 根据地表多角度数据提取 BRDF 原型

从 2.2.2 节的分析中我们可以看出,AFX 较好地指示地表基本散射类型的变化,如果将其作为 BRDF 特征的分类指标,建立一个体现 BRDF 变化的 BRDF 原型库 (每个 BRDF 形状代表特定波段不重复的 BRDF 形状的变化,因此该形状称为 BRDF

原型),可能会有助于 BRDF 作为地表先验知识的应用。为提取地表 BRDF 原型,首先根据核驱动模型拟合地面多角度数据得到模型参数,根据模型参数计算每组数据的 AFX,然后再用迭代自组织数据分析技术(ISODATA)对 AFX 进行分类,并将每一类内相应的模型参数的均值作为 BRDF 原型库中该类原型的模型参数。最后,为了便于更直观地显示和对比,还需要对模型参数进行光谱归一化处理,在这里也将各向同性参数归一化到 0.5。

为了确定最佳的原型个数,我们将数据分成 2—9 类,用每一类得到的模型参数去拟合类内的观测数据,并计算平均拟合误差。研究表明,随着原型数目的增加,拟合误差均值和标准差都逐渐减小,当原型数大于 4 时,下降趋势趋于平缓,红波段的拟合误差保持在 0.018 附近,近红外波段保持在 0.04 附近,考虑到算法的复杂度及结果的精度,最终在红和近红外波段分别建立了包含 4 种 BRDF 原型的原型库。根据多角度数据建立 BRDF 原型库的具体方法可参考 Jiao 等人(2012)。表 1 给出了每一类内所有数据 AFX 的均值及原型在光谱归一化前后的模型参数值。原型在主平面上的形状,如图 3 所示,从下到上分别对应表 1 中 R1—R4 或 N1—N4。从中可以清楚的看到,随着 AFX 数值的增大,Fvol 逐渐增大,Fgeo 逐渐减小,即几何光学作用逐渐减弱,体散射效应逐渐增强,BRDF 原型由“屋顶状”过渡到“碗状”。

表 1 根据 AFX 对地表观测数据分类后得到每一类 AFX 均值 AFX_{mean}、BRDF 原型参数及光谱归一化后的原型参数

	类别	AFX_{mean}	f_{iso}	f_{vol}	f_{geo}	F_{iso}	F_{vol}	F_{geo}
红波段	R1	0.6714	0.2040	0.0690	0.0552	0.5	0.1724	0.1429
	R2	0.8916	0.1341	0.0338	0.0160	0.5	0.1868	0.0650
	R3	1.0060	0.0899	0.0571	0.0079	0.5	0.3875	0.0511
	R4	1.2412	0.0391	0.0526	0.0010	0.5	0.7097	0.0099
近红外波段	N1	0.6855	0.3713	0.1023	0.0995	0.5	0.1508	0.1349
	N2	0.9202	0.2857	0.1021	0.0311	0.5	0.2048	0.0571
	N3	1.0460	0.3168	0.1855	0.0149	0.5	0.3097	0.0258
	N4	1.1808	0.3390	0.3261	0.0006	0.5	0.4881	0.0014

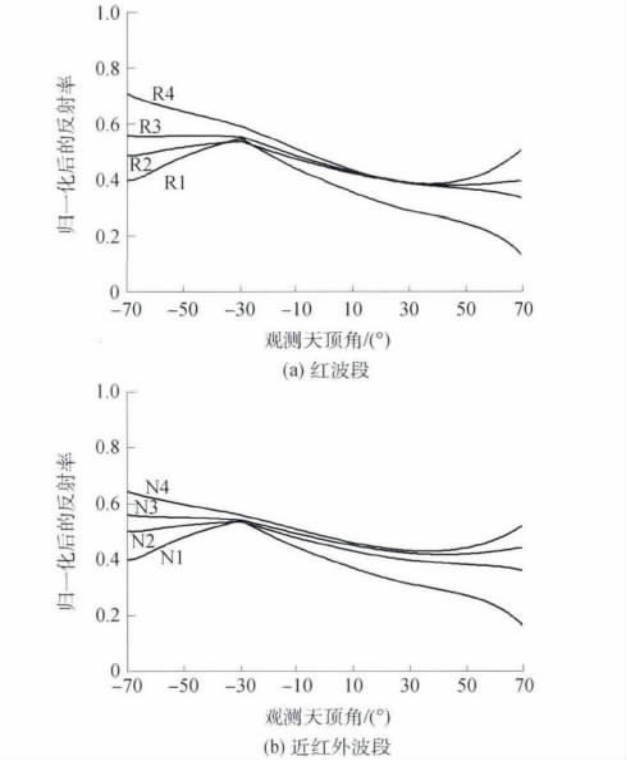

图 3 太阳天顶角为 30°时,红波段和近红外波段的 4 种 BRDF 原型在主平面上的形状

3 原型反演算法及验证

3.1 原型反演算法

BRDF 原型对地表各向异性特征进行了有效地概括,多角度数据在以 BRDF 原型为先验知识反演地表反照率时,利用各原型分别去拟合观测数据,根据拟合误差选择最优的原型,这是本文 BRDF 原型反演的基本思想。具体反演过程如下:假定一组有 n 个观测的多角度观测数据 $\boldsymbol{B}$: $\boldsymbol{B}=\rho_0(\boldsymbol{\Omega}_{i,0};\boldsymbol{\Omega}_{r,0})$, $\rho_1(\boldsymbol{\Omega}_{i,1};\boldsymbol{\Omega}_{r,1}),\cdots,\rho_{n-1}(\boldsymbol{\Omega}_{i,n-1};\boldsymbol{\Omega}_{r,n-1})$,假设已知与其对应的 BRDF 原型为 BRDF′,它在数据 $\boldsymbol{B}$ 的观测位置对应的原型反射率数据为 $\boldsymbol{B}'$: $\boldsymbol{B}'=\rho'_0(\boldsymbol{\Omega}_{i,0};\boldsymbol{\Omega}_{r,0})$, $\rho'_1(\boldsymbol{\Omega}_{i,1};\boldsymbol{\Omega}_{r,1}),\cdots,\rho'_{n-1}(\boldsymbol{\Omega}_{i,n-1};\boldsymbol{\Omega}_{r,n-1})$,取调整系数 a,通过平移 BRDF 原型,使得 $\boldsymbol{B}$ 和 $a\boldsymbol{B}'$ 的差异最小,采用最小二乘拟合法最小化拟合误差 e^2(Strugnell 和 Lucht,2001):

$$e^2=\sum_{i=0}^{n-1}(\rho_i-a\rho'_i)^2 \tag{4}$$

求调整系数 a,

$$a = \frac{\sum_{j=0}^{n-1} \rho_j \times \rho_j'}{\sum_{j=0}^{n-1} (\rho_j')^2} \tag{5}$$

这样，数据 B 的 BRDF 就可以表示为：

$$\mathrm{BRDF} = a \times \mathrm{BRDF} \tag{6}$$

拟合误差 RMSE 可以表示为

$$\mathrm{RMSE} = \sqrt{\frac{1}{n-1} \sum_{k=0}^{n-1} (\rho_k - a\rho_k')^2} \tag{7}$$

用 4 种原型分别拟合观测数据，计算每一种原型的拟合误差 RMSE，然后选择拟合观测数据最优的原型，即 RMSE 最小的 BRDF 原型作为数据的先验 BRDF，然后就可以通过式(5)确定调整系数 a，那么黑天空 BSA 和白天空 WSA 反照率与选定的最优原型的黑天空 BSA′和白天空 WSA′反照率之间的关系可以表示为：

$$\mathrm{BSA}(\theta,\lambda) = a \times \mathrm{BSA}'(\theta,\lambda) = a \times \sum_k F_k(\lambda) h_k(\theta) \tag{8}$$

$$\mathrm{WSA}(\lambda) = a \times \mathrm{WSA}'(\lambda) = a \times \sum_k (F_k(\lambda) H_k) \tag{9}$$

式中，$h_k(\theta)$ 是相应的核在观测半球的积分值，它们是太阳天顶角的函数；H_k 是核在入射和观测半球的积分值，他们与角度无关是一个定值，在 RossThick 和 LiSparseR 对应的积分值分别是 0.189184 和 −1.137762。

3.2 BRDF 原型反演算法验证

地表反射的各向异性特征在主平面上表现的更为显著，而在垂直主平面上各向异性特征则相对平缓(Li 和 Strahler，1992)。从图 2 和图 3 中我们也可以看出，当地物的各向异性较强时(AFX 较大或较小时)，主平面上的反射率随着观测角度的不同而有明显差异，在后向“热点”处有一个峰值，在前向“冷点”处有一个低谷，在大的观测天顶角处变化也十分显著。同时我们从图 2 中还可以看出，地物各向异性对地物反射量的大小的影响作用与地物光谱量的大小有关，图 2 中小麦的 AFX 为 1.24，体散射效应显著，但其真实反射率的大小分布在 0.05—0.1，而当将其光谱量归一化到 0.5 以后，其反射率分布在 0.3—0.75，即当地物的光谱量越大，各向异性作用导致地表各个方向反射量的差异也越大。但在垂直主平面上，随着观测天顶角的变化，地物的承照面和阴影的比例相对稳定，因此反射率并不会表现出明显的“热点”及“冷点”效应，BRDF 形状变化平缓。

为评价算法的精度，首先结合 BRDF 的上述特征以及地表多角度数据的角度分布特征，从数据中选择位于主平面，垂直主平面，以及与主平面夹角为 30°和 60°的平面上，且观测天顶角小于 40°的观测数据子集作为验证数据。用全反演算法和原型反演算法分别拟合验证数据得到地表反照率，再与全反演算法拟合完整数据集得到的验证参考值作比较。每组验证数据的观测数目为 4—12 个，并且这些观测都有相同的太阳天顶角，基本对应 MODIS 业务化产品的备用算法 (Jin 等，2003) 的范畴，验证数据可以较好地代表观测信息不足的情况。完整数据集是在多个太阳天顶角下收集的，所以对于同一数据集，可以选出多组满足上述条件的验证数据集。

将原型反演算法及全反演算法拟合验证数据集得到白天空反照率与验证参考值进行比较，对比散点图如图 4 所示，结果反演精度如表 2 所示。从对比结果可以看出：(1) 当选定的观测位于非垂直主平面时，原型反演算法在红波段的反照率与验证参考值的最小决定系数在 0.944，而全反演算法与验证参考值的决定系数最大为 0.927，两种算法的最大平均相对误差在 60°平面处获得，分别为 17.14% 和 27.63%，原型反演算法较全反演算法的相对精度提高约 5%—10%，在近红外波段有相似的结果，结果精度提高约 3%—8%。(2) 当观测位于垂直主平面时，在红和近红外波段，全反演的结果与真实值的决定系数均约为 0.36，最大平均绝对差异高达 0.18，而原型反演的结果与真实值的最大平均绝对和相对差异为 0.037 和 13.52%。(3) 对于验证数据子集，全反演在红和近红外波段分别有 17 组和 26 组数据反演失败(反照率大于 1 或小于 0)，图 4 中空心圆和空心三角形分别表示全反演的结果失败和与反照率真实值的差异大于 0.1 时原型反演算法的结果，可以看出虽然全反演结果失败或差异较大，但原型的反演的结果均在精度要求范围以内。综上所述，在多角度观测信息量不足的情况下，原型反演算法的精度要高于全反演算法，这种优势在垂直主平面上表现的尤为显著。

基于核驱动模型的全反演算法对多角度观测数据的数量，角度分布及观测噪声均有较严格的限制(Jin 等，2003；Shuai 等，2008)，原型反演算法以全反演算法为基础，借助于先验知识在采样空间内对 BRDF 进行了约束。本研究中选用的验证数据子集的观测天顶角集中在 40°内，从而缺乏大的观测天

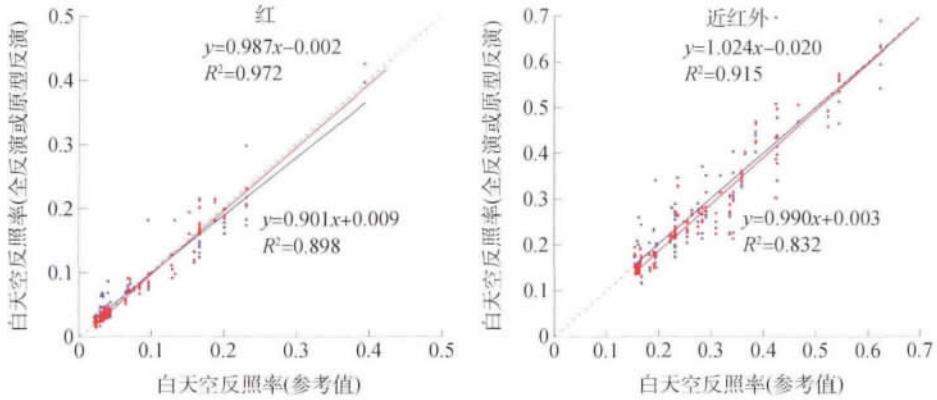

(a) 观测位于主平面上的验证数据集(样本总量102组)

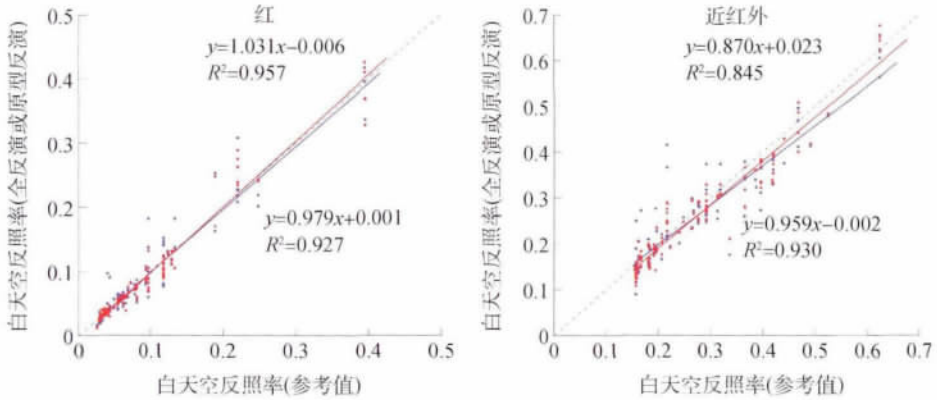

(b) 观测位于30°平面(103组)

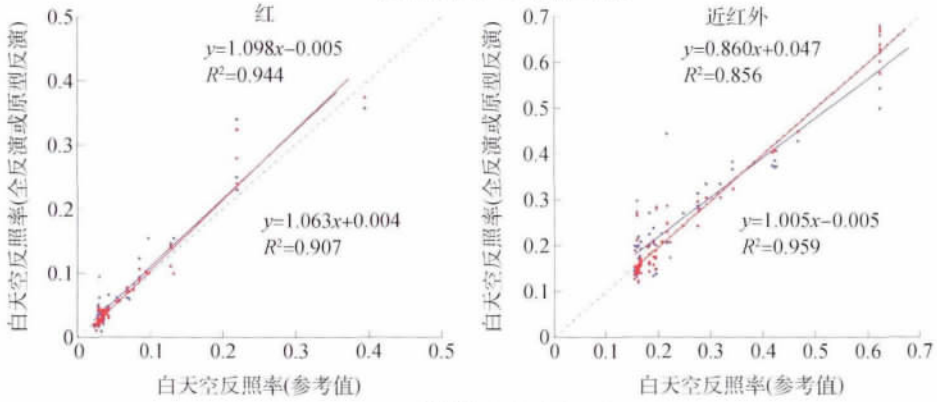

(c) 观测位于60°平面(57组)

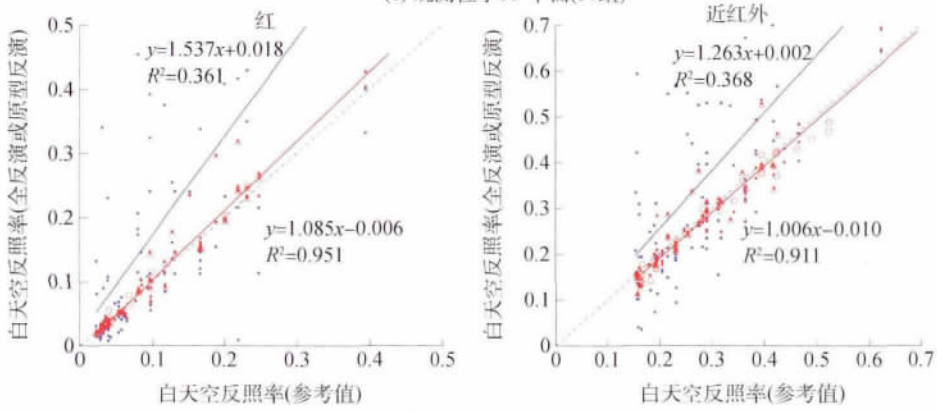

(d) 观测位于垂直主平面(121组)

图4 全反演算法与原型反演算法拟合不同平面上验证数据得到的白天空反照率与验证参考值的对比图

(红色表示原型反演算法,蓝色表示全反演算法。空心圆和空心三角形分别表示全反演算法的结果失败或与真实值的差异大于0.1的数据)

表 2 原型反演算法结果精度表

波段	平面	RMSE1	RMSE2	ε_1/%	ε_2/%
红波段	PP	0.02325	0.01217	21.630	11.906
	30P	0.02272	0.01834	17.483	12.681
	60P	0.02382	0.01862	27.631	17.135
	CP	0.18281	0.02173	99.306	13.515
近红外波段	PP	0.04667	0.03325	13.791	9.440
	30P	0.05007	0.03555	13.287	10.227
	60P	0.05733	0.03100	18.574	10.872
	CP	0.18469	0.03692	46.921	9.760

注：RMSE1、ε_1 和 RMSE2、ε_2 分别为全反演结果或原型反演结果与真实值的绝对和相对差异，PP、30P、60P 和 CP 分别表示主平面、与主平面夹角为 30°或 60°平面、垂直主平面。

顶角下的约束，当观测位于主平面时，验证数据集在一定程度上代表了地表的各向异性，当观测位于垂直主平面时，观测数据集的地表各向异性代表性变弱。因此，全反演算法及原型反演算法在主平面上基本能够取得较为一致的反演结果，但原型反演算法的结果略优于全反演算法，随着采样平面逐渐远离主平面（从 30°平面，到 60°平面，最后到垂直主平面），全反演结果精度表现出快速下降趋势，甚至会出现异常的情况。然而，基于 BRDF 原型的原型反演算法变化很小，表明该算法即使在观测数据较少且采样分布相对集中的情况下，对地表反照率反演依然有着很好的稳定性。需要说明的是在 60°平面上原型反演算法结果精度稍微偏低，这可能与验证数据子集对地表各向异性的代表性有关，也可能与验证数据子集的样本数量有关，在此平面上验证数据有 57 组，而另外 3 个平面验证数据在 100 组以上。综上所述，类似于本文中的验证数据，当多角度观测数据方向信息量不足时，原型反演算法通过对 BRDF 原型先验知识的应用，可以较为精确地描述地表的各向异性特征，得到较精确的反演地表反照率，尤其当观测数据角度分布不理想时，原型反演算法的优势更加显著。

为了更清晰地说明在多角度数据信息量不足时，原型反演算法较全反演算法的优势，我们从验证数据集中选择了 4 组位于主平面或垂直主面上验证数据集进行分析。图 5 分别表示主平面或垂直主平面上的 BRDF 形状及相应的观测数据，表 3 给出了相应的白天空反照率结果及两种算法与验证参考值的绝对差异。可以看出，当选择的观测数据位于主平面时，观测数据能够在一定程度上体现地表的各向异性特征，原型反演和全反演算法都能够取得较精确的结果（图 5（a））；受数据的角度分布及噪声的影响，此时原型反演算法的精度略优于全反演算法；当观测数据中存在明显的噪声，同时在大的观测天顶角及热点处缺乏观测时，全反演的结果会变的不稳定，导致结果有较大的偏差（图 5（b））；当观测位于垂直主平面上时，观测数据对地表各向异性特征的代表性不强，再加上缺乏大角度下的观测数据以及受到观测噪声的影响，往往会导致全反演算法在大角度下反演的结果异常，最终导致反演结果存在较大差异甚至失败（图 5（a）（b））。原型反演算法引入了 BRDF 原型作为先验知识，在整个空间范围内对 BRDF 进行了硬性约束，对观测数据角度分布的依赖性相对较小，抗噪声的能力较强，在观测信息缺失的情况下，依然能够获得与真实情况较接近的地表反照率。而目前各种传感器的多角度采样能力都十分有限，因此原型反演算法也有着广阔的应用前景。

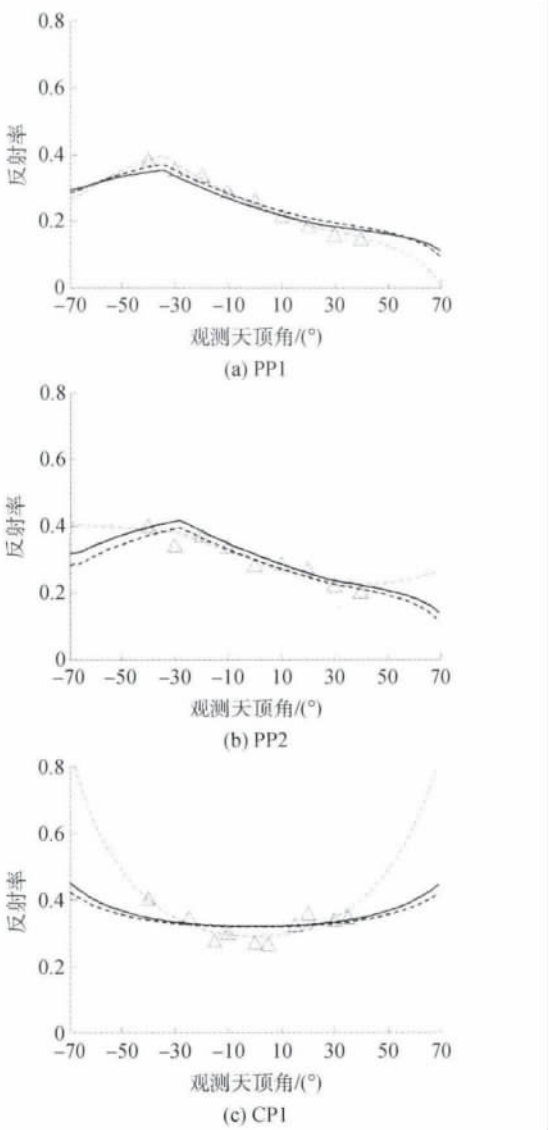

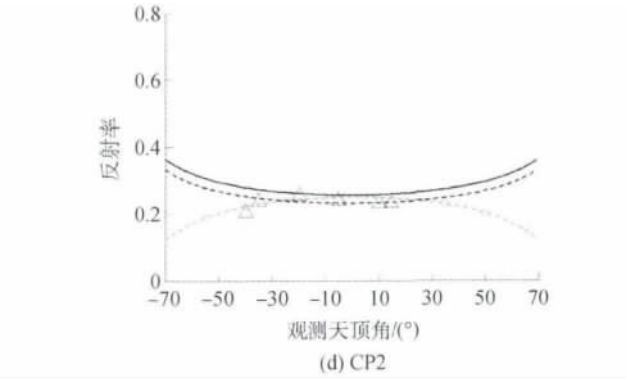

图5 验证数据分布图及相应的BRDF形状
(黑色实线代表真实的BRDF形状,黑色虚线代表原型反演的结果,灰色虚线代表全反演的结果,三角形表示观测数据,PP和CP分别代表观测数据位于主平面和垂直主平面)

表3 图5中对应4组验证数据的白天空反照率及绝对差异

	WSA_T	WSA_F	WSA_A	D_{ft}	D_{at}
PP1	0.23157	0.19388	0.22671	0.0377	0.0049
PP2	0.28360	0.37039	0.25294	0.0868	0.0307
CP1	0.41742	0.70213	0.39599	0.2847	0.0214
CP2	0.29094	0.21124	0.27212	0.0797	0.0188

注:WSA_T代表为验证参考值,WSA_F代表全反演,WSA_A代表原型反演,D_{ft}、D_{at}分别代表全反演或原型反演与验证参考值的绝对差异。

4 结 论

根据AFX对地表各向异性反射的指示作用,通过对地表多角度观测数据集分类后建立了BRDF原型库,提出了基于BRDF原型反演地表反照率的算法,并根据模拟的观测天顶角分布范围较小、观测信息不足的数据子集对原型算法进行了验证,对比了全反演算法和原型反演算法结果的精度差异,并对造成差异的原因进行了分析。本研究对利用地表先验知识反演地表反照率提供了新的有益尝试,对根据观测信息不足的多角度数据反照率的反演具有重要意义。研究得到的主要结论如下:

(1) AFX对地表反射各向异性特征的变化起到指示作用,随着AFX数值的增大,体散射效应逐渐增强,几何光学作用逐渐减弱。通过AFX对地表数据分类后建立的BRDF原型,从整体上概括了地表的各向异性特征,为地表先验知识的利用提供了新思路。

(2) 先验知识能够有效地解决遥感反演中信息量不足的问题,原型反演算法的优势是能够在整个空间范围内对BRDF进行了先验约束,在借助先验知识的同时又有效地利用了观测数据的各向异信息,使其在观测数据有限的情况下仍能够较精确地反演地表反照率。

(3) 原型反演算法和MODIS全反演算法相比,当观测数据较少或角度分布不理想时,原型反演算法具有更高的精度和稳定性,但其对观测角度的数量,位置分布以及观测数据的质量的要求较全反演算法要低。通常情况下,原型反演算法的相对精度比全反演算法高3%—10%,当观测数据位于垂直主平面时,原型反演算法的优势更加明显。

在本研究中用到的地表多角度数据大多在植被生长旺盛的季节获得,忽略了季节变化对BRDF的影响作用。为获取更具有代表性的先验BRDF原型,先验数据还需要进一步扩充和完善,下一步将在先验知识中添加POLDER数据及全球EOS站点的MODIS数据,分析原型算法的适用条件和BRDF原型的尺度效应,研究地表各向异性的季节性差异及BRDF原型的波段相关性,为观测信息量不足的多角度数据的地表各向异性校正和多角度观测的星载传感器的反照率反演提供有意义的参考。

参考文献(References)

Bacour C and Bréon F M. 2005. Variability of biome reflectance directional signatures as seen by POLDER. Remote Sensing of Environment, 98(1): 80 - 95 [DOI: 10.1016/j.rse.2005.06.008]

Dickinson R E. 1983. Land surface processes and climate surface albedos and energy balance. Advances in Geophysics, 25: 305 - 353 [DOI: 10.1016/S0065 - 2687(08)60176 - 4]

Deering D W and Leone P. 1986. A sphere-scanning radiometer for rapid directional measurements of sky and ground radiance. Remote Sensing of Environment, 19(1): 1 - 24 [DOI: 10.1016/0034 - 4257(86)90038 - 6]

Deering D W, Eck T F and Grier T. 1992. Shinnery oak bidirectional reflectance properties and canopy model inversion. IEEE Transactions on Geoscience and Remote Sensing, 30(2): 339 - 348 [DOI: 10.1109/36.134083]

Dickinson R E. 1995. Land processes in climate models. Remote Sensing of Environment, 51(1): 27 - 38 [DOI: 10.1016/0034 - 4257(94)00062 - R]

Deering D W, Eck T F and Banerjee B. 1999. Characterization of the reflectance anisotropy of three boreal forest canopies in spring-summer. Remote Sensing of Environment, 67(2): 205 - 229 [DOI: 10.1016/S0034 - 4257(98)00087 - X]

Hu B X, Lucht W, Li X W and Strahler A H. 1997. Validation of kernel-drives semiempirical models for the surface bidirectional reflectance distribution function of land surfaces. Remote Sensing of Environment, 62(3): 201 - 214

Huang X，Jiao Z，Dong Y，Zhang H and Li X. 2013. Analysis of BRDF and albedo retrieved by kernel-driven models using field measurements. IEEE Journal of Selected Topics in Applied Earth Observations and Remote Sensing，6(1)：149 - 161 [DOI：10.1109/JSTARS.2012.2208264]

Irons J R，Campbell G S，Norman J M，Graham D W and Kovalick W M. 1992. Prediction and measurement of soil bidirectional reflectance. IEEE Transactions on Geoscience and Remote Sensing，30(2)：249 - 260 [DOI：10.1109/36.134075]

焦子锑，李小文，王锦地，张虎. 2011. **评估 MODIS 的 BRDF 角度指数产品. 遥感学报**，15(3)：432 - 456

Jiao Z，Zhang H and Li X W. 2012. To derive a prior database of archetypal BRDF shapes from ground measurements using anisotropic flat index (AFX) // Proceedings of the IEEE International Geoscience and Remote Sensing Symposium (IGARSS). Munich：IEEE：6753 - 6756 [DOI：10.1109/IGARSS.2012.6352555]

Jin Y F，Schaaf C B，Woodcock C E，Gao F，Li X W，Strahler A H，Lucht W and Liang S. 2003. Consistency of MODIS surface bidirectional reflectance distribution function and albedo retrievals：1. Algorithm performance. Journal of Geophysical Research-Atmospheres，108(D5)：4158 [DOI：10.1029/2002JD002803]

Kimes D S. 1983. Dynamics of directional reflectance factor distributions for vegetation canopies. Applied Optics，22(9)：1364 - 1372 [DOI：10.1364/AO.22.001364]

Kimes D S，Newcomb W W，Nelson R F and Schutt J B. 1986. Directional reflectance distributions of a hardwood and pine forest canopy. IEEE Transactions on Geoscience and Remote Sensing，G E-24(2)：281 - 293

Leroy M and Breon F M. 1996. Angular signatures of surface reflectances from airborne POLDER data. Remote Sensing of Environment，57(2)：97 - 107 [DOI：10.1016/0034 - 4257(95)00229 - 4]

Lewis P and Barnsley M J. 1994. Influence of the sky radiance distribution on various formulations of the earth surface albedo // Proc. Conf. Phys. Meas. Sign. Remote Sens.，Val d'Isere，France：707 - 715

Li X and Strahler A H. 1992. Geometric-optical bidirectional reflectance modeling of the discrete crown vegetation canopy：effect of crown shape and mutual shadowing. IEEE Transactions on Geoscience and Remote Sensing，30(2)：276 - 292 [DOI：10.1109/36.134078]

李小文，王锦地. 1995. **植被光学遥感模型与植被结构参数化. 北京：科学出版社**

Li X and Strahler A H. 1985. Geometric-optical modeling of a conifer forest canopy. IEEE Transactions on Geoscience and Remote Sensing，GE-23(5)：705 - 721 [DOI：10.1109/TGRS.1985.289389]

Li X W，Gao F，Wang J D and Strahler A. 2001. A priori knowledge accumulation and its application to linear BRDF model inversion. Journal of Geophysical Research：Atmospheres，106(D11)：11925 - 11935 [DOI：10.1029/2000JD900639]

Liu J，Schaaf C，Strahler A，Jiao Z T，Shuai Y，Zhang Q L，Roman M，Augustine J A and Dutton E G. 2009. Validation of Moderate Resolution Imaging Spectroradiometer (MODIS) albedo retrieval algorithm：Dependence of albedo on solar zenith angle. Journal Geophysical Reserarch，114 (D1)：D01106 [DOI：10.1029/2008JD009969]

Lucht W，Schaaf C B and Strahler A H. 2000. An algorithm for the retrieval of albedo from space using semiempirical BRDF models. IEEE Transactions on Geoscience and Remote Sensing，38(2)：977 - 998 [DOI：10.1109/36.841980]

Nicodemus F E，Richmond J C，Hsia J J，Ginsberg I W and Limperis T. 1977. Geometrical Considerations and Nomenclature for Reflectance. Washington，DC：National Bureau of Standards，US Department of Commerce

Ranson K J，Biehl L L and Bauer M E. 1985. Variation in spectral response of soybeans with respect to illumination，view and canopy geometry. International Journal of Remote Sensing，6(12)：1827 - 1842 [DOI:10.1080/01431168508948331]

Roman M O Gatebe C K，Schaaf C B，Poudyal R，Wang Z S and King M D. 2011. Variability in surface BRDF at different spatial scales (30 m—500 m) over a mixed agricultural landscape as retrieved from airborne and satellite spectral measurements. Remote Sensing of Environment，115(9)：2184 - 2203 [DOI：10.1016/j.rse.2011.04.012]

Roujean J L，Leroy M and Deschamps P Y. 1992. A bidirectional reflectance model of the Earth's surface for the correction of remote sensing data. Journal of Geophysical Research，97(D18)：20455 - 20468 [DOI：10.1029/92JD01411]

Schaaf C B，Gao G，Strahler A H，Lucht W，Li X，Tsang T，Strugnell N C，Zhang X，Jin Y，Muller J P，Lewis P，Barnsely M J，Hobson P，Disney M，Roberts G，Dunderdale M，Doll C，D'Entremont R P，Hu B，Liang S，Privette J and Roy D P. 2002. First operational BRDF，albedo nadir reflectance products from MODIS. Remote Sensing of Environment，83(1/2)：135 - 148 [DOI：10.1016/S0034 - 4257(02)00083 - 4]

Shuai Y，Schaaf C B，Strahler A H，Liu J and Jiao Z. 2008. Quality assessment of BRDF/albedo retrievals in MODIS operational system. Geophysical Research Letters，35 (5) [DOI：10.1029/2007GL032568]

Strahler A H and Jupp D L B. 1990. Bidirectional reflectance modeling of forest canopies using boolean models and geometric optics // Proceedings of Remote Sensing Science for the Nineties'，10th Annual International. Geoscience and Remote Sensing Symposium. USA：IEEE：1751 - 1755 [DOI：10.1109/IGARSS.1990.688854]

Strugnell N C and Lucht W. 2001. An algorithm to infer continental-scale albedo from AVHRR data，land cover class，and field observations of typical BRDFs. Journal of Climate，14(7)：1360 - 1376 [DOI：10.1175/1520 - 0442(2001)014<1360：AATICS>2.0.CO;2]

Tsay S C，King M D，Arnold G T and Li J Y. 1998. Airborne spectral measurements of surface anisotropy during SCAR-B. Journal of Geophysical Research-Atmospheres，103(D24)：31943 - 31953

Vierling L A，Deering D W and Eck T F. 1997. Differences in arctic tundra vegetation type and phenology as seen using bidirectional radiometry in the early growing season. Remote Sensing of Environment，60(1)：71 - 82 [DOI：10.1016/S0034 - 4257(96)00139 - 3]

Wanner W，Li X and Strahler A H. 1995. On the derivation of kernels for kernel-driven models of bidirectional reflectance. Journal of Geophysical Research，100(D10)：21077 - 21089 [DOI：10.1029/95JD02371]